radiations. This behavior is attributed to the mixing of Hg 5d character with the σ_g bonding level.[28] Because the cross section of the Hg 5d level is the only atomic cross section which increases significantly between these energies, the rapid decrease in p cross section is offset by Hg 5d orbital mixing. This same behavior has recently been observed in the valence band of mercuric dihalides, and similar conclusions have been made.[28] In addition to these observations, the splitting patterns of the Hg 5d levels[1,2,10] are further confirmation of the slight bonding nature of the Hg 5d orbitals.

Acknowledgment. We are very grateful to the NSERC (Canada) for financial support, to R. Lazier for excellent technical support, to Dr. S. Stobart for kindly supplying the $(Me_3SiCH_2)_2Cd$, and to J. S. Tse for helpful discussions.

Registry No. Me_2Zn, 544-97-8; Et_2Zn, 557-20-0; Me_2Cd, 506-82-1; Et_2Cd, 592-02-9; n-Pr_2Cd, 5905-48-6; $(Me_3SiCH_2)_2Cd$, 63835-91-6; Me_2Hg, 593-74-8; Et_2Hg, 627-44-1.

Contribution from the Department of Chemistry, Northern Illinois University, DeKalb, Illinois 60115

Electronic Structure and Spectra of Linear Dihaloaurate(I) Ions

MARY E. KOUTEK and W. ROY MASON*

Received August 29, 1979

Solution absorption and magnetic circular dichroism (MCD) spectra in the ultraviolet region are reported for $[(n\text{-}C_4H_9)_4N][AuX_2]$ (X = Cl^-, Br^-, and I^-) in CH_3CN. Absorption spectra are also reported for unoriented crystalline films of these compounds on quartz plates at 300 and 26 K, with considerable resolution enhancement observed for $AuBr_2^-$ and AuI_2^- at low temperature. The $AuCl_2^-$ spectra are interpreted in terms of a parity forbidden 5d → 6s transition and allowed 5d → 6p transitions, while the spectra of $AuBr_2^-$ and AuI_2^- exhibit in addition ligand to metal charge-transfer (LMCT) transitions. The LMCT spectra for AuI_2^- are interpreted by means of excited configurations which include both ligand and metal spin–orbit coupling. Detailed spectral assignments are presented and the results discussed in terms of gold orbital participation in bonding and the extent of halide to gold σ and π bonding in the AuX_2^- ions.

Introduction

Gold(I) forms some of the best examples of linear two-coordinate complexes which can be considered as prototypes of this very simple coordination geometry. Consequently electronic spectra of linear two-coordinate Au(I) complexes are of interest in providing an experimental basis for the study of electronic structure of two-coordination in general. However, except for the $Au(CN)_2^-$ ion, whose spectra have been studied in some detail,[1,2] little is known about electronic spectra of two-coordinate gold(I) complexes. This may be partly due to experimental difficulties encountered with many Au(I) complexes in aqueous solution. For example, simple dihalo complexes, AuX_2^- (X = Cl^-, Br^-, and I^-), are unstable with respect to disproportionation in aqueous solution.[3] Many other complexes containing P, S, or As donor ligands are simply not soluble; those that are disproportionate or hydrolyze. Although some of these problems may be avoided by the use of nonaqueous solvents, molecular Au(I) complexes generally exhibit spectra in the UV region which have often been obscured by strong ligand or counterion absorptions.[4,5]

As part of a systematic investigation of electronic spectra of two-coordinate Au(I) complexes, the present paper reports spectral measurements for the dihaloaurate(I) complexes, $AuCl_2^-$, $AuBr_2^-$, and AuI_2^-. Simple discrete linear ions are presumed for these three complexes, analogous to isoelectronic HgX_2 (X = Cl^-, Br^-, and I^-) complexes which are known to be linear. Structural studies of AuX_2^- salts are limited,[5,6] but in each case linear two-coordination about the gold is indicated. Infrared and Raman spectra have been interpreted in terms of ions of $D_{\infty h}$ symmetry,[3,7] and single ^{35}Cl and ^{37}Cl nuclear quadrupole resonances are observed for $AuCl_2^-$, indicating equivalent chloride ligands.[7,8] Previous electronic spectral measurements for AuX_2^- in acetonitrile, although incomplete, revealed a single weak band (ϵ <250) for each complex, which was assigned to a parity forbidden 5d → 6s transition.[9] In the present paper we report acetonitrile solution spectra for tetra-n-butylammonium salts of $AuCl_2^-$, $AuBr_2^-$, and AuI_2^-, which extend to the high-energy solvent cutoff (5.1 μm^{-1}). In addition, magnetic circular dichroism (MCD) spectra were obtained for acetonitrile solutions. Spectra were also recorded for thin crystalline films of the tetra-n-butylammonium salts on quartz plates at 300 and 26 K.

Experimental Section

The tetra-n-butylammonium dihaloaurate(I) salts, $[(n\text{-}C_4H_9)_4N][AuX_2]$, where X = Cl^-, Br^-, and I^-, were prepared by the methods described by Braunstein and Clark.[3] Excellent yields of the dibromo and diiodo complexes were obtained, but difficulties were encountered with the synthesis of the dichloro complex via phenylhydrazine hydrochloride reduction of $[(n\text{-}C_4H_9)_4N][AuCl_4]$ in ethanol. Only small amounts of product were obtained in each of several experiments. In several other cases the product was severely contaminated with either unreacted starting material or gold metal. Attempts to improve the synthesis by changing the reducing agent or solvent were unsuccessful. However, enough pure product was obtained from multiple preparations for analysis and spectral measurements. All three compounds gave satisfactory elemental analysis.

Absorption spectral measurements were made by using a Cary Model 1501. Spectroquality acetonitrile was used throughout for solution spectra. The MCD spectra were recorded on a JASCO

(1) Mason, W. R. *J. Am. Chem. Soc.* **1973**, *95*, 3573.
(2) Mason, W. R. *J. Am. Chem. Soc.* **1976**, *98*, 5182.
(3) Braunstein, P.; Clark, R. J. H. *J. Chem. Soc., Dalton Trans.* **1973**, 1845.
(4) Brown, D. H.; McKinlay, G.; Smith, W. E. *J. Chem. Soc. Dalton Trans.* **1977**, 1874.
(5) Beurskens, P. T.; Blaauw, H. J. A.; Cras, J. A.; Steggerda, J. J. *Inorg. Chem.* **1968**, *7*, 805.
(6) Tindemans van Eijndhoven, J. C. M.; Verschoor, G. C. *Mater. Res. Bull.* **1974**, *9*, 1667.
(7) Bowmaker, G. A.; Whiting, R. *Aust. J. Chem.* **1976**, *29*, 1407.
(8) Jones, P. G.; Williams, A. F. *J. Chem. Soc., Dalton Trans.* **1977**, 1430.
(9) Roulet, R.; Lan, N. Q.; Mason, W. R.; Fenske, G. P. *Helv. Chim. Acta* **1973**, *56*, 2405.

0020-1669/80/1319-0648$01.00/0

Table I. Basis Functions

irreducible representn	metal orbitals	ligand combinatns
σ_g^+	d_{z^2}, s	$(1/2)^{1/2}(\sigma_1 + \sigma_2)$
σ_u^+	p_z	$(1/2)^{1/2}(\sigma_1 - \sigma_2)$
π_g^x	d_{yz}	$-(1/2)^{1/2}(\pi_{y1} + \pi_{y2})$
π_g^y	$-d_{xz}$	$(1/2)^{1/2}(\pi_{x1} - \pi_{x2})$
π_u^x	p_x	$(1/2)^{1/2}(\pi_{x1} + \pi_{x2})$
π_u^y	p_y	$(1/2)^{1/2}(\pi_{y1} - \pi_{y2})$
δ_g^θ	$d_{x^2-y^2}$	
δ_g^ϵ	d_{xy}	

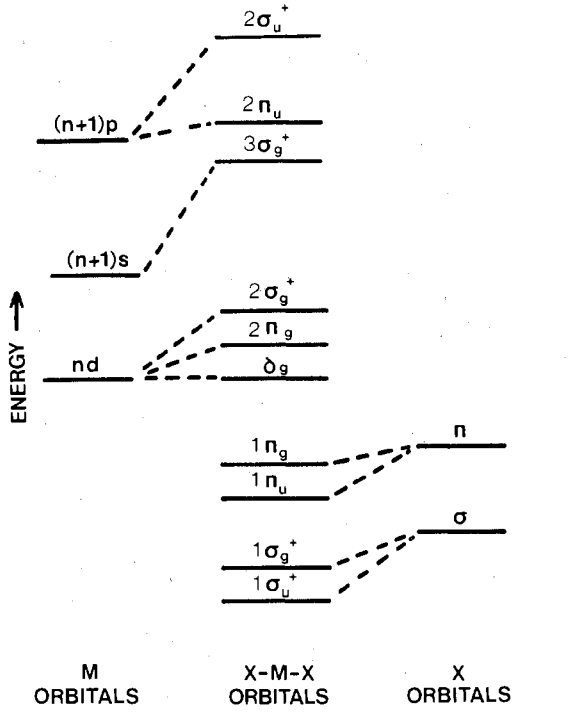

Figure 1. Molecular orbital energy levels for a linear ($D_{\infty h}$) MX_2^{n-} complex.

ORD/UV-5 (equipped with a CD attachment) using a permanent magnet (field 1.0 T). Low-temperature spectra were obtained by using a Cryo-Tip hydrogen refrigerator (Air Products and Chemicals, Inc.); temperatures below 100 K were measured by using a calibrated gallium arsenide diode. The preparation of the thin crystalline films on quartz plates has been described previously.[2]

Some absorption spectra were also obtained for comparison purposes for cyclohexane (spectroquality) solutions of reagent grade mercury(II) chloride, bromide and iodide.

Molecular Orbital Energy Levels

A suitable coordinate system for the linear AuX_2^- complexes is given below

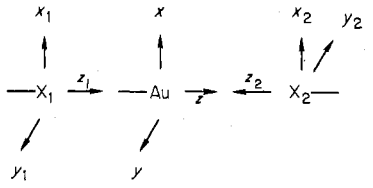

while metal and ligand orbital basis functions are listed in Table I. The σ_i and π_i functions are sp_z hybrids and p_x or p_y atomic orbitals, respectively, on the halide. A generalized one-electron molecular orbital energy level scheme for linear dihalo complexes is presented in Figure 1. Since Au(I) has a $5d^{10}$ electronic configuration, the highest filled level is $2\sigma_g^+$ in the figure. The electronic ground state is nondegenerate, diamagnetic, and totally symmetric, designated $^1\Sigma_g^+$. Dipole selection rules restrict fully allowed transitions to $^1\Sigma_u^+$ (z polarized) or $^1\Pi_u$ (x,y polarized) excited states since r transforms as $\sigma_u^+(z)$ and $\pi_u(x,y)$ in $D_{\infty h}$ molecules. However, in heavy-metal complexes spin-selection rules may breakdown due to spin–orbit coupling, and transitions to formally spin-forbidden triplet excited states may gain appreciable intensity by admixtures of $^1\Sigma_u^+$ and $^1\Pi_u$ states.

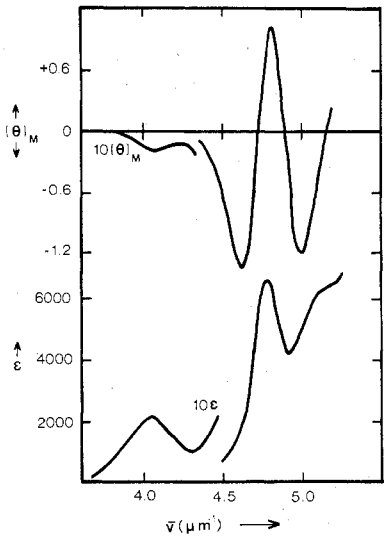

Figure 2. Electronic absorption (lower curves) and magnetic circular dichroism (upper curves) of $[(n\text{-}C_4H_9)_4N][AuCl_2]$ in CH_3CN solution.

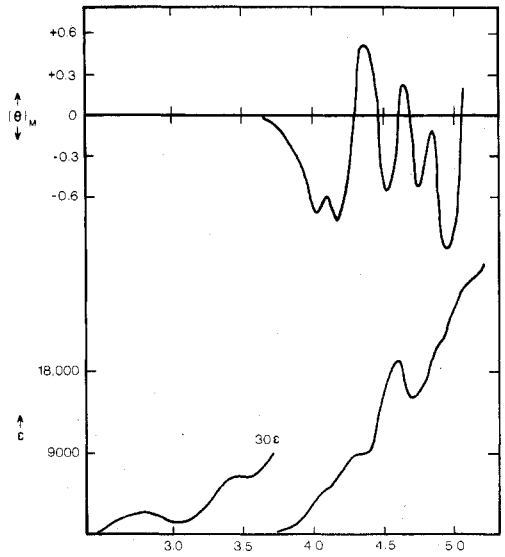

Figure 3. Electronic absorption (lower curves) and magnetic circular dichroism (upper curve) of $[(n\text{-}C_4H_9)_4N][AuI_2]$ in CH_3CN solution.

Results and Discussion

Electronic Absorption and MCD Spectra. Figures 2 and 3 present absorption and MCD spectra for $AuCl_2^-$ and AuI_2^- in acetonitrile solution. The spectra of $AuBr_2^-$ were of comparable quality. For all three complexes weak absorptions ($\epsilon \lesssim 215$) were found at lower energy, which compare favorably with the spectra reported previously.[9] Associated with these weak bands, broad weak *B* terms were observed in the MCD for $AuCl_2^-$ and $AuBr_2^-$, but the MCD in the region of the weak bands for AuI_2^- was too weak to obtain reliable data, even though nearly saturated solutions were employed. At higher energy more intense band systems ($\epsilon > 2000$) were observed for all three complexes, with one or more *A* terms observed in the MCD spectra. In all three cases the absorption spectra obeyed Beer's law over a 5–10-fold concentration range.

Figures 4 and 5 present solid-state spectra for thin crystalline samples (unoriented) of $[(n\text{-}C_4H_9)_4N][AuBr_2]$ and $[(n$-

Table II. Electronic Spectral Data for AuX_2^-

band no.	crystal: 300 K $\bar{\nu}$, μm^{-1} (rel abs)[a]	crystal: 26 K $\bar{\nu}$, μm^{-1} (rel abs)[a]	solution[b]: abs $\bar{\nu}$, μm^{-1} (ϵ, M^{-1} cm^{-1})	solution[b]: MCD $\bar{\nu}$, μm^{-1} ($[\theta]_M$)[c]	assignment: state	assignment: [configurtn][d]
			$[(n\text{-}C_4H_9)_4N][AuCl_2]$			
1	4.08 (0.096)	4.20 (0.037) 4.80 (0.63)[e] 4.85 (0.73)[e]	4.06 (212)	4.06 (−0.018)	Σ_g^+	$[(2\sigma_g^+)(3\sigma_g^+)]$
2	4.87 (1.00)	4.92 (0.85) 5.07 (0.45)	4.78 (6600)	*f*: 4.65 (−1.3); 4.72 (0); 4.81 (+1.04)	Π_u	$[(2\sigma_g^+)(2\pi_u)]$
			5.10 (6200)[e]	*f*: 5.00 (−1.22); 5.15 (0); *g*	Π_u	$[(\delta_g)^3(2\pi_u)]$
			$[(n\text{-}C_4H_9)_4N][AuBr_2]$			
1	3.94 (0.037)	4.03 (0.020)	3.90 (152)	3.91 (−0.018)	Σ_g^+	$[(2\sigma_g^+)(3\sigma_g^+)]$
2	4.62 (0.36)[e]	4.62 (0.25)	4.44 (2600)[e]	4.42 (−0.35)[e]	$\Pi_u(^3\Pi_u)$	$[(1\pi_u)^3(3\sigma_g^+)]$
3	4.83 (0.85)	4.78 (0.85)	4.72 (10 600)	*f*: 4.60 (−1.84); 4.69 (0); 4.74 (+0.52)	Π_u	$[(2\sigma_g^+)(2\pi_u)]$
4		4.86 (0.83)			$\Pi_u(^1\Pi_u)$	$[(1\pi_u)^3(3\sigma_g^+)]$
5	5.10 (0.93)	5.14 (1.00)	4.96 (11 200)	*f*: 4.90 (−0.65); 5.00 (0); *g*	Π_u	$[(\delta_g)^3(2\pi_u)]$
			$[(n\text{-}C_4H_9)_4N][AuI_2]$			
1	2.82 (0.021)	2.82 (0.033)	2.77 (78)	*h*	$\Sigma_u^+(^3\Sigma_u^-)$	$[(1\pi_g)^3(2\pi_u)]$
2		3.15 (0.017)[e]			Π_g	$[(1\pi_g)^3(3\sigma_g^+)]$
3	3.42 (0.047)[e]	3.48 (0.060)	3.48 (210)	*h*	$\Pi_u(^3\Pi_u)$	$[(1\pi_u)^3(3\sigma_g^+)]$
4		3.80 (0.046)			Σ_g^+	$[(2\sigma_g^+)(3\sigma_g^+)]$
5	4.15 (0.24)[e]	4.15 (0.26)	4.10 (4900)[e]	4.02 (−0.72)	$\Sigma_u^-(^1\Sigma_u^+)$	$[(1\pi_g)^3(2\pi_u)]$
6	4.35 (0.32)	4.25 (0.26)[e]	4.32 (8800)[e]	*f*: 4.17 (−0.79); 4.29 (0); 4.35 (+0.52)	$\Pi_u(^1\Pi_u)$	$[(1\pi_u)^3(3\sigma_g^+)]$
7		4.43 (0.35)			$\Pi_u(^3\Pi_u)$	$[(1\sigma_g^+)(2\pi_u)]$
8	4.65 (0.48)	4.64 (0.55)	4.58 (19 200)	*f*: 4.52 (−0.54); 4.61 (0); 4.63 (+0.23)	Π_u	$[(2\sigma_g^+)(2\pi_u)]$
9		4.84 (0.54)[e]		4.74 (−0.52)	Σ_g^+, Σ_g^-, Δ_g	$[(1\pi_u)^3(2\pi_u)]$
10	4.95 (0.83)[e]	4.97 (0.92)[e]	4.90 (21 600)[e]	*f*: 4.94 (−0.98); 5.05 (0); *g*	Π_u	$[(\delta_g)^3(2\pi_u)]$
11		5.03 (1.00)			$\Pi_u(^1\Pi_u)$	$[(1\sigma_g^+)(2\pi_u)]$

[a] Relative absorbance. [b] CH_3CN, 300 K. [c] $3300(\Delta A)/(HlC)$, ΔA = differential absorbance, H = magnetic field in gauss, l = path length in cm, C = molar concentration. [d] Orbitals labeled as in Figure 1; filled orbitals omitted. [e] Shoulder. [f] *A* term. [g] Ellipticity becomes positive, but signal to noise was too low to obtain reliable information. [h] MCD signal too weak for reliable measurement.

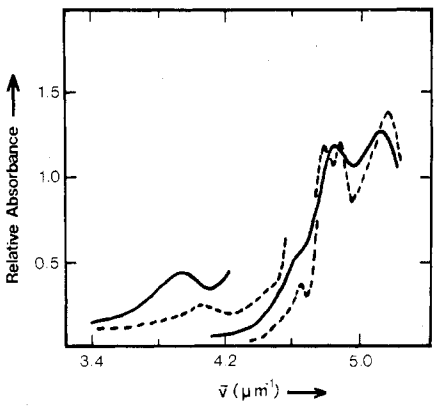

Figure 4. Electronic absorption spectra of crystalline $[(n\text{-}C_4H_9)_4N][AuBr_2]$ on quartz: (—) 300 K; (---) 26 K. The spectra on the left were obtained for a thicker sample than the spectra on the right.

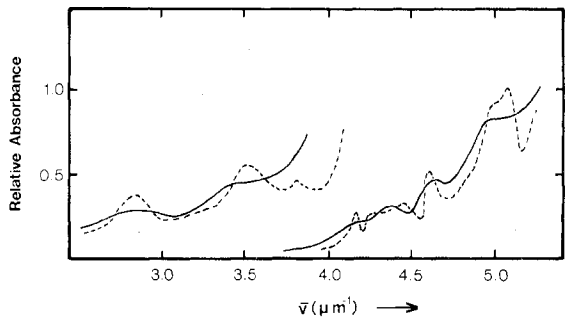

Figure 5. Electronic absorption spectra of crystalline $[(n\text{-}C_4H_9)_4N][AuI_2]$ on quartz: (—) 300 K; (---) 26 K. The spectra on the left were obtained for a thicker sample than the spectra on the right.

$C_4H_9)_4N][AuI_2]$ on quartz plates at 300 and 26 K. Samples of different thickness were necessary to record data for both the weak bands at low energy and the more intense bands at higher energy. Considerable enhancement of resolution is observed at low temperature. The changes in the spectra of the bromo and iodo complexes on cooling were completely reversible. Spectra were also obtained for crystalline samples of $[(n\text{-}C_4H_9)_4N][AuCl_2]$, but some differences were observed on cooling. The temperature dependence of the low-energy, low-intensity band at 4.1 μm^{-1} was similar to that observed for corresponding bands in the bromo and iodo complexes. In contrast to the results for the bromo and iodo complexes, the area under the intense absorption band at 4.9 μm^{-1} decreased on cooling, which is not typical of allowed charge-transfer bands. Further, the changes in the spectra of the chloro complex on cooling were not reversible in the region of the intense band. The origin of this anomalous behavior for the $[(n\text{-}C_4H_9)_4N][AuCl_2]$ samples on cooling is not known; the changes in the spectra may be due to an irreversible crystal phase change.

Quantitative spectral data for both solution and solid-state measurements are collected in Table II.

Spectral Assignments. Before detailed band assignments can be made for the AuX_2^- spectra, the excited electronic configuration associated with each transition must be iden-

Table III. Electronic Spectral Data for HgX_2

vapor phase[a] $\bar{\nu}$, μm^{-1} (ϵ, M^{-1} cm^{-1})	cyclohexane solution $\bar{\nu}$, μm^{-1} (ϵ, M^{-1} cm^{-1})	assignmt
	$HgCl_2$	
5.00 (2300)	5.00 (0.75)[b]	π-LMCT
	$HgBr_2$	
4.35 (1400)	4.25 (2700)	π-LMCT
5.00 (3400)	5.05 (16 300)	σ-LMCT
	HgI_2	
3.73 (3600)	3.64 (4300)	π-LMCT
4.47 (6500)	4.47 (12 600)	σ-LMCT
4.81 (3300)		σ-LMCT?

[a] Data from ref 11. [b] Absorbance of a saturated solution; low solubility precluded accurate ϵ determination.

tified. Referring to Figure 1, three types of excited configurations are expected at lowest energy for linear dihalo complexes. These configurations are (1) d → s configurations in which a metal *n*d electron is excited to the metal $(n + 1)$s $(3\sigma_g^+)$ orbital, (2) d → p configurations in which a metal *n*d electron is excited to the metal $(n + 1)$p $(2\pi_u)$ orbitals, and (3) ligand to metal charge-transfer (LMCT) configurations in which an electron is excited from a halide-based π orbital $(1\pi_g$ or $1\pi_u)$ or σ orbital $(1\sigma_g^+$ or $1\sigma_u^+)$ to the metal $(n + 1)$s $(3\sigma_g^+)$ or metal $(n + 1)$p $(2\pi_u)$ orbitals. The first two types of excitations involve predominantly metal orbitals and therefore their energies should show only weak dependence on the nature of the ligands. The d → s transitions are parity forbidden and are expected to be quite weak. In contrast to the d → s and d → p transitions, the energies of the LMCT transitions are expected to be strongly ligand dependent with their order parallel to the ligand orbital stabilities, viz., $Cl^- > Br^- > I^-$. Further, transitions involving the ligand $1\pi_g$ or $1\pi_u$ orbitals (π-LMCT) are expected at lower energy than those involving the $1\sigma_g^+$ or $1\sigma_u^+$ orbitals (σ-LMCT).

Allowed LMCT and d → p transitions may be differentiated by comparing the spectra of the AuX_2^- complexes with isoelectronic HgX_2 complexes. The LMCT process is sensitive to metal orbital stability and is expected to red shift as the metal oxidation state is increased from Au(I) to Hg(II). In contrast, examination of atomic spectral data[10] shows that the d → p excited configurations (d → s also) shift to higher energy from Au(I) to Hg(II). Therefore to provide data for comparison purposes, we investigated the spectra of $HgCl_2$, $HgBr_2$, and HgI_2 briefly. Table III collects the results of our measurements in cyclohexane solution and some data for the vapor phase.[11] Attempts were made to obtain solution spectra for the mercury(II) halides in acetonitrile, but the spectra obtained did not obey Beer's law and band shapes were highly concentration dependent. Considerable solvent dependence has been observed for the mercury(II) halides in a number of unsaturated organic solvents, which has been attributed to intermolecular association between solvent and complex.[12] In acetonitrile solvolysis may also be responsible for the observed spectral changes. Further study of the mercury(II) halide spectra in acetonitrile are necessary to clarify their behavior. The intense bands observed in the UV region for the mercury(II) halides have been assigned as halide to metal LMCT,[11,13] though detailed assignments have not been discussed. The LMCT assignment is supported by photoelectron spectra for $HgCl_2$, $HgBr_2$, and HgI_2 which show that the highest occupied orbitals (lowest energy ionizations) are halide orbitals.[14] The lowest energy band for the mercury(II) halides assigned to π-LMCT (Table III) shows the expected halide-dependent energy $Cl^- > Br^- > I^-$. Higher energy σ-LMCT bands are also observed in $HgBr_2$ and HgI_2.

Turning now to the spectra of the AuX_2^- ions, Table II sets forth band assignments for each complex. The rationale for these assignments is discussed for each complex in turn.

$AuCl_2^-$. The lowest energy intense band for the $AuCl_2^-$ complex is observed at 4.8 μm^{-1} (band 2) and is *lower* in energy than the lowest energy band in $HgCl_2$. This observation rules out LMCT for the $AuCl_2^-$ spectra. Also charge transfer to solvent (CTTS)[15] in acetonitrile solutions of $AuCl_2^-$, and the other dihalo Au(I) complexes, can be ruled out since the solution and solid spectra are quite similar. The intense bands in the $AuCl_2^-$ spectra at 4.8 and 5.1 μm^{-1} are therefore logically assigned as d → p transitions. Atomic spectral data show that the d → p assignments are reasonable on energetic grounds since $5d^96p$ configurations range from 4.2 to 6.3 μm^{-1} for charges on Au between 0 and +1.[10] The observation of positive *A* terms in the MCD for bands 2 and 3 of $AuCl_2^-$ is consistent with the assignment of these bands to the allowed Π_u states corresponding to $2\sigma_g^+ \rightarrow 2\pi_u$ (band 2) and $\delta_g \rightarrow 2\pi_u$ (band 3); positive *A* terms are predicted for both of these transitions if the orbitals involved are approximated as pure atomic orbitals. In view of the irreversible changes that are observed for band 2 on cooling, a more detailed interpretation of the structure observed for this band at low temperatures is probably not warranted here. The weak band at 4.1 μm^{-1} (band 1) is assigned as the parity forbidden d → s transition $2\sigma_g^+ \rightarrow 3\sigma_g^+$. The temperature dependence of this band indicates a vibronically allowed transition.

$AuBr_2^-$. The intense bands 3 and 5 have nearly the same energy as the d → p transitions assigned for $AuCl_2^-$. The similarity in energy argues for an analogous d → p assignment for $AuBr_2^-$. The MCD spectra also show two positive *A* terms for these bands so that assignment to the allowed Π_u states corresponding to $2\sigma_g^+ \rightarrow 2\pi_u$ (band 3) and $\delta_g \rightarrow 2\pi_u$ (band 5) is reasonable.

At low temperature a band is resolved at 4.86 μm^{-1} (band 4). This band is *higher* in energy than the lowest energy LMCT in $HgBr_2$ at 4.25 μm^{-1} in cyclohexane solution (Table III) and therefore may be assigned as an allowed π-LMCT. Since the low-resolution MCD spectra show only a positive *A* term in the region of bands 3 and 4, it is probable that both bands have unresolved overlapping positive *A* terms associated with them. The allowed Π_u state corresponding to $1\pi_u \rightarrow 3\sigma_g^+$ is predicted to have a positive *A* term if the $1\pi_u$ orbitals are approximated as halide p_x and p_y atomic orbitals and therefore the MCD is not inconsistent with the π-LMCT assignment of band 4. An alternative assignment of band 4 to the d → p transition $2\pi_g \rightarrow 2\pi_u$ is considered unlikely since the allowed excited state would be Σ_u^+ and would mix strongly with the d → p Π_u states in the presence of a magnetic field and therefore should show a definite *B* term on the high-energy side of the *A* term for band 3.

Band 1 is a weak band which is vibronically allowed, analogous to the lowest energy band observed for $AuCl_2^-$. The energy of this band is shifted only slightly to lower energy from the analogous band in the $AuCl_2^-$ spectrum. Thus this band is assigned to the d → s transition $2\sigma_g^+ \rightarrow 3\sigma_g^+$.

Band 2 observed both at 300 K as a shoulder and resolved as a maximum at 26 K has no counterpart in the $AuCl_2^-$ spectrum. The energy of band 2 is 0.24 μm^{-1} lower than band

(10) Moore, C. E. "Atomic Energy Levels". *Natl. Bur. Stand. (U.S.) Circ.* **1958**, No. 467, Vol. III.
(11) Templet, P.; McDonald, J. R.; McGlynn, S. P.; Kendrow, C. H.; Roebber, J. L.; Weiss, K. *J. Chem. Phys.* **1972**, *56*, 5746.
(12) Eliezer, I.; Avinur, P. *J. Chem. Soc., Faraday Trans. 2* **1974**, *70*, 1316.
(13) Spiro, T. G.; Hume, D. N. *J. Am. Chem. Soc.* **1961**, *83*, 4305.
(14) Eland, J. H. D. *Int. J. Mass Spectrom. Ion Phys.* **1970**, *4*, 37.
(15) El-Kourasky, A; Grinter, R. *J. Chem. Soc., Faraday Trans. 2* **1977**, *73*, 1050.

Table IV. Spin-Orbit Matrices for Excited LMCT Configurations[a]

π-LMCT

$\Pi_u\ [(1\pi_u)^3(3\sigma_g^+)]^b$

$$\begin{vmatrix} {}^1\Pi_u - E & \frac{i}{2}\zeta_{np}(X) \\ -\frac{i}{2}\zeta_{np}(X) & {}^3\Pi_u - E \end{vmatrix}$$

$\Sigma_u^+\ [(1\pi_g)^3(2\pi_u)]^b$

$$\begin{vmatrix} {}^1\Sigma_u^+ - E & -\frac{i}{2}[\zeta_{np}(X) + \zeta_{6p}(Au)] \\ \frac{i}{2}[\zeta_{np}(X) + \zeta_{6p}(Au)] & {}^3\Sigma_u^- - E \end{vmatrix}$$

σ-LMCT

$\Pi_u\ [(1\sigma_g^+)(2\pi_u)]^b$

$$\begin{vmatrix} {}^1\Pi_u - E & -\frac{i}{2}\zeta_{6p}(Au) \\ \frac{i}{2}\zeta_{6p}(Au) & {}^3\Pi_u - E \end{vmatrix}$$

[a] $\zeta_{np}(X)$ is the spin-orbit coupling parameter for the ligand X; $\zeta_{6p}(Au)$ is the spin-orbit coupling parameter for the gold 6p orbitals. The singlet and triplet states along the diagonals are excited states of the indicated symmetry in the absence of spin-orbit coupling. [b] Excited LMCT configurations (filled orbitals omitted); see Figure 1 for orbital notation.

4 assigned to an allowed LMCT. Consideration of spin–orbit coupling (for details, see the treatment for AuI_2^- later) indicates that the Π_u states from the $^1\Pi_u$ and $^3\Pi_u$ states arising from the $(1\pi_u)^3 3\sigma_g^+$ configuration will mix strongly with their separation due to spin–orbit interaction being approximately $\zeta_{4p}(Br^-)$, the spin–orbit coupling constant for the ligand ($\zeta_{4p}(Br) \simeq 0.25\ \mu m^{-1}$).[16] Thus band 2 may be assigned as a transition to the formally spin forbidden $^3\Pi_u$ state, which has gained intensity by spin–orbit mixing with the higher energy $^1\Pi_u$ state. An alternative assignment of band 2 might be to another d → s transition $2\pi_g \rightarrow 3\sigma_g^+$ or $\delta_g \rightarrow 3\sigma_g^+$. However, the relative intensity (ϵ 2600) is rather high for a parity forbidden transition. Further, if the transition is d → s, then a corresponding band should be observed for $AuCl_2^-$. No such band was resolved.

AuI_2^-. The most striking feature of the AuI_2^- spectra compared to the $AuBr_2^-$ and $AuCl_2^-$ spectra is the larger number of bands, especially those resolved at low temperature. Also, the weak low-energy bands 1 and 3 have different temperature dependence and are much lower in energy than the weak d → s bands of $AuBr_2^-$ and $AuCl_2^-$. These spectral differences can be rationalized in terms of the low-energy shift expected for the I^- LMCT spectra compared to Br^- and Cl^- and the increased importance of spin–orbit coupling due to the ligand ($\zeta_{5p}(I) \simeq 0.50\ \mu m^{-1}$).[16] The intense d → p bands and the weak d → s band identified in the $AuCl_2^-$ and $AuBr_2^-$ spectra persist essentially unaffected for AuI_2^- (bands 10, 8, and 4, respectively), although the d → s transition is resolved only at low temperature. The remaining bands in the AuI_2^- spectrum are assigned to LMCT. Because of the increased spin–orbit interaction in AuI_2^-, the formally spin-forbidden LMCT transitions gain intensity and shift to lower energy than the d → s transition. In order to serve as a guide for spectral assignments as well as provide insight into the mixing of LMCT excited states, we gave a qualitative consideration to intraconfigurational spin–orbit interaction in the LMCT configurations. By the approximation of the ligand $1\sigma_g^+$, $1\pi_u$ and $1\pi_g$ orbitals as atomic 5p orbitals on I^- and the $3\sigma_g^+$ and $2\pi_u$ orbitals as 6s and 6p atomic orbitals on the gold, spin–orbit matrices were developed for allowed σ- and π-LMCT states. These matrices are given in Table IV, where the excited singlet and triplet states in the absence of spin–orbit coupling are given along the diagonals. The spin–orbit parameters $\zeta_{np}(X)$ and $\zeta_{6p}(Au)$ refer to the I^- 5p and the gold 6p orbitals, respectively. Thus the $\Pi_u(^1\Pi_u)$ and $\Pi_u(^3\Pi_u)$ spin–orbit states of $(1\pi_u)^3(3\sigma_g^+)$ depend upon $\zeta_{5p}(I^-)$, while those of $(1\sigma_g^+)(2\pi_u)$ depend upon $\zeta_{6p}(Au)$. The $\Sigma_u^+(^1\Sigma_u^+)$ and $\Sigma_u^+(^3\Sigma_u^-)$ spin–orbit states of $(1\pi_g)^3(2\pi_u)$ depend upon both $\zeta_{5p}(I^-)$ and $\zeta_{6p}(Au)$. Some simple calculations were performed by using estimates of the energies of the singlet and triplet LMCT states and values for $\zeta_{5p}(I^-)$[16] and $\zeta_{6p}(Au)$.[17] The results are compared with the experimental 26 K spectra in Figure 6. The positions of the d → s and d → p bands are indicated for comparison. Also included in Figure 6 are parity forbidden π-LMCT assignments for two poorly defined shoulders at 3.15 and 4.84 μm^{-1} (bands 2 and 9) resolved at 26 K. The assignments indicated in Figure 6 are summarized in Table II.

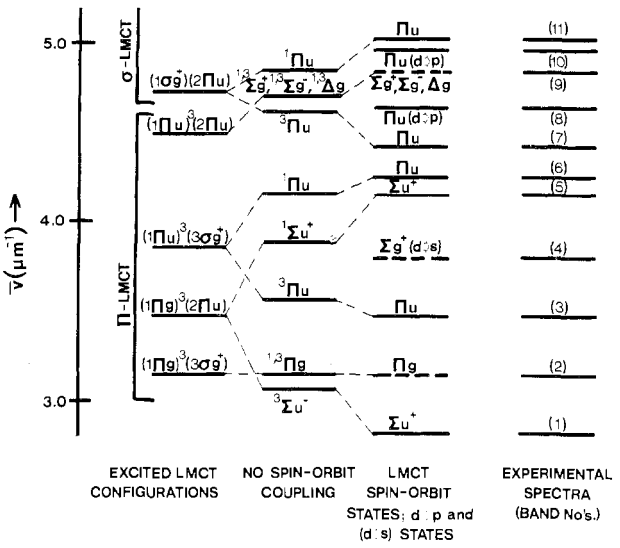

Figure 6. Spin–orbit states for LMCT configurations, together with d → p and d → s excited states, compared with experimental spectra. Input parameters for the spin–orbit calculations (in μm^{-1}): $\zeta_{5p}(I) = 0.5$; $\zeta_{6p}(Au) = 0.55$; $^1\Pi_u(\sigma\text{-LMCT}) = 4.85$; $^3\Pi_u(\sigma\text{-LMCT}) = 4.62$; $^1\Pi_u(\pi\text{-LMCT}) = 4.16$; $^3\Pi_u(\pi\text{-LMCT}) = 3.57$; $^1\Sigma_u^+ = 3.89$; $^3\Sigma_u^- = 3.08$; (---) parity forbidden.

Electronic Structure and Bonding in AuX_2^-. The spectral assignments given in Table II provide a self-consistent interpretation of the AuX_2^- spectra in which the relative energies of the LMCT transitions shift to lower energies relative to the d → p and d → s transitions as X^- is changed from Cl^- to Br^- to I^-. It is noteworthy that while LMCT transitions are common for transition-metal–halide complexes, there have been few other examples of d → s and d → p transitions observed for metal complexes. An allowed d → p band was reported for the planar $Pt(NH_3)_4^{2+}$ ion,[18,19] a 3d → 4p transition has been identified for Cu(I) in alkali halide crystals,[20] and 4d → 5s transitions were suggested for weak bands observed for Ag(I) aquo ions.[21] Gold(I) complexes are probably among the best complexes in which to observe these metal interorbital transitions because the $5d^96s$ and $5d^96p$ configu-

(16) Jørgensen, C. K. *Mol. Phys.* **1959**, *2*, 309.

(17) ζ_{6p} is expected to be larger than ζ_{5d}; see: Griffith, J. S. "The Theory of Transition Metal Ions"; Cambridge University Press: London, 1964; Chapter 5 and Table A6.3.

(18) Mason, W. R.; Gray, H. B. *J. Am. Chem. Soc.* **1968**, *90*, 5721.

(19) Isci, H.; Mason, W. R. *Inorg. Nucl. Chem. Lett.* **1972**, *8*, 885.

(20) Simonetti, J.; McClure, D. S. *Phys. Rev. B* **1977**, *16*, 3887.

(21) Jørgensen, C. K. "Absorption Spectra and Chemical Bonding in Complexes"; Addison-Wesley: Reading, MA, 1962; p 201.

rations of Au(I) lie at relatively low energies compared to other metal ions.[10]

The spectral assignments for AuX_2^- can provide information not only on the relative energies of excited states but also on orbital participation in bonding. The assignments of the d → p bands in all three complexes indicate an orbital energy ordering of $2\sigma_g^+ > \delta_g$, but the separation of the two d → p transitions is relatively small ranging from 0.24 to 0.32 μm^{-1}. Apart from differences in electron repulsions, this small separation suggests only a small difference in energy between the σ-antibonding $2\sigma_g^+$ orbital and the nonbonding δ_g orbitals and thus a very low participation of the $5d_z^2$ orbital in σ bonding. Although the d → p transition from the $2\pi_g$ orbitals was not located, the $2\pi_g$ orbitals are expected to be more weakly antibonding than the $2\sigma_g^+$ and to be located energetically between the $2\sigma_g^+$ and δ_g orbitals. A similar conclusion concerning the involvement of the Au 5d orbitals in bonding was drawn from the detailed study of the $Au(CN)_2^-$ spectra where only a small 5d orbital splitting was inferred.[2] The small splitting of the Au 5d orbitals may therefore be regarded as a general feature of two-coordinate Au(I) complexes since it is found for such widely different ligands as CN^- and halides. Since the filled 5d orbitals are presumed to have little involvement, the main contributions to bonding in two-coordinate Au(I) complexes must rest with the empty 6s and 6p orbitals. The $3\sigma_g^+$ and $2\sigma_u^+$ are expected to be strongly σ antibonding and thus may be visualized as forming the basis for two sp_z hybrid orbitals on Au. The use of sp_z hybrid orbitals on Au to describe the bonding in linear two-coordinate Au(I) complexes has received considerable support recently from ^{197}Au Mössbauer studies.[22-25] The large isomer shift (s-orbital participation) and quadrupole splitting (p_z-orbital participation) observed for a variety of Au(I) complexes both increase with the donor strength of the ligand. This observation can be explained easily in terms of sp_z hybridization of Au but appears to be inconsistent with an earlier proposal involving $d_{z^2}s$ hybridization.[26]

The lack of 5d orbital participation tends to rule out significant halide → 5d π bonding so that the $1\pi_g$ ligand orbitals should be virtually nonbonding. Further, the observation of d → p transitions in AuX_2^- at energies anticipated from atomic spectral data[10] for the free ion strongly suggests that halide → 6p π bonding is weak. Strong π bonding involving the 6p orbitals on Au would be expected to destabilize $2\pi_u$ considerably and thus shift d → p transitions to higher energy. This conclusion is further supported by photoelectron spectra of HgX_2 which suggest only a small (but not zero) degree of halide → 6p π bonding in these compounds.[14] π donation from halide ligands to Au(I) is expected to be less than for Hg(II) due to the lower charge on the metal. Thus the contribution to the overall bonding in AuX_2^- from halide to metal π bonding is expected to be small. Consequently σ bonding must be the dominant type of bonding in these complexes and primarily responsible for their stability.

Because of a lack of information concerning relative differences in electron repulsions, it is difficult to draw firm conclusions from the relative energies of the LMCT excited states for $AuBr_2^-$ and AuI_2^-. However, the pattern of LMCT bands observed for AuI_2^- indicates approximately 0.8 μm^{-1} energy difference between the π-LMCT and σ-LMCT band systems. This difference is comparable to that found for HgI_2 (0.74 μm^{-1}) and $HgBr_2$ (0.65 μm^{-1}) but is somewhat smaller than found for typical square-planar MX_4^{n-} or octahedral MX_6^{n-} halide complexes.[18,27,28] As noted earlier[28] this difference between the σ- and π-LMCT can be viewed qualitatively as a "ligand field splitting" of the energies of the *np* halide orbitals by the metal ion. However, as shown here in Figure 6 the splitting magnitude observed in the electronic spectra also depends upon electron repulsion and spin–orbit coupling differences between the excited states involving the σ- and π-donor orbitals—differences which may be considerable for heavy-metal ions and Br^- or I^- ligands.

Registry No. $[(n\text{-}C_4H_9)_4N][AuCl_2]$, 50480-99-4; $[(n\text{-}C_4H_9)_4N][AuBr_2]$, 50481-01-1; $[(n\text{-}C_4H_9)_4N][AuI_2]$, 50481-03-3; $HgCl_2$, 7487-94-7; $HgBr_2$, 7789-47-1; HgI_2, 7774-29-0.

(22) Faltens, M. O.; Shirley, D. A. *J. Chem. Phys.* **1970**, *53*, 4249.
(23) Charlton, J. S.; Nichols, D. I. *J. Chem. Soc. A* **1970**, 1484.
(24) McAuliffe, C. A.; Parish, R. V.; Randall, P. D. *J. Chem. Soc., Dalton Trans.* **1977**, 1426.
(25) Jones, P. G.; Maddock, A. G.; Mays, M. J.; Muir, M. M.; Williams, A. F. *J. Chem. Soc., Dalton Trans.* **1977**, 1434.
(26) Orgel, L. E. *J. Chem. Soc.* **1958**, 4186. Dunitz, J. D.; Orgel, L. E. *Adv. Inorg. Chem. Radiochem.* **1960**, *2*, 1.
(27) Swihart, D. L.; Mason, W. R. *Inorg. Chem.* **1970**, *9*, 1749.
(28) Blanchard, W. D.; Mason, W. R. *Inorg. Chim. Acta* **1978**, *28*, 159.

Contribution from the Department of Chemistry, University College, Cardiff, Wales, United Kingdom

Angular-Overlap Calculation of the Jahn–Teller Stabilization Energies for f-Orbital Degeneracies

KEITH D. WARREN

Received March 29, 1979

The angular-overlap model is applied to the calculation of the linear Jahn–Teller coupling constants for f-orbital degeneracies. The MX_6, O_h, chromophore is treated as representative of the highest symmetry commonly occurring in the lanthanide and actinide series, and it is shown that, even when spin–orbit effects are taken into account, 5f orbital degeneracies may lead to significant Jahn–Teller stabilization energies. The operation of this effect for f^1 Γ_8 states is considered.

Introduction

In 1971 Jørgensen[1] could, with some justification, note that although many f^x systems were in principle Jahn–Teller active, there was no convincing experimental evidence for the operation of the effect in such species. Thus Eisenstein and Pryce[2] had earlier suggested that the higher Γ_8' excited state of the $5f^1$ NpF_6 system could show Jahn–Teller splitting, and evidence for such activity had also been adduced[3] for the $5f^2$ U^{4+}

(1) C. K. Jørgensen, "Modern Aspects of Ligand Field Theory", North-Holland Publishing Co., Amsterdam, 1971.
(2) J. C. Eisenstein and M. H. L. Pryce, *Proc. R. Soc. London, Ser. A*, **255**, 181 (1960).
(3) K. Sasaki and Y. Obata, *J. Phys. Soc. Jpn.*, **28**, 1157 (1970).

0020-1669/80/1319-0653$01.00/0